Asociación Argentina
de Mecánica Computacional

Mecánica Computacional Vol XXIX, págs. 2581-2598 (artículo completo)
Eduardo Dvorkin, Marcela Goldschmit, Mario Storti (Eds.)
Buenos Aires, Argentina, 15-18 Noviembre 2010

SOUND SCATTERING OPTIMIZATION USING THE TOPOLOGICAL DERIVATIVE AND THE BOUNDARY ELEMENT METHOD

Agustín Sisamon[a], Silja C. Beck[b], Adrián P. Cisilino[a] and Sabine Langer[b]

[a]*INTEMA, Universidad Nacional de Mar del Plata – CONICET, Av. Juan B. Justo 4302, 7600 Mar del Plata, Argentina, cisilino@fi.mdp.edu.ar, http://www.intema.gov.ar*

[b]*Institut für Angewandte Mechanik, Technische Universität Braunschweig, Spielmannstr. 11, 38106 Braunschweig, Germany, infaminfo@tu-bs.de, http://www.infam.bau.tu-bs.de*

Keywords: Topological Derivative, Iterative Optimization, Acoustic Scattering.

Abstract. Today, reduction of sound emission plays a vital role while designing objects of any kind. Desirable aspects might include decreased radiation in certain directions of such an object. This work shows an approach to iteratively compute the shape of an obstacle which fulfils best to prescribed design variables using the framework provided by the topological derivative and the boundary element method (BEM).

At the beginning of the process a design space is defined in which in iterative steps the shape will be developed. A regular array of points is set over the entire design space. The objective function is given by a set of prescribed pressure values for the scatter pattern on a circle around this design space.

The object, which acts as a scatterer, is considered acoustically rigid. The shape of the object builds up cumulatively, adding in each iterative step a rigid inclusion at the position that the topological derivative identifies as the most effective to achieve the prescribed design values. The procedure is repeated until a given stopping criteria is satisfied. The proposed method requires the computation of a forward problem and an adjoint problem for each step. The first is solved using a standard BEM for 2D acoustics, while the latter is solved backwards using the prescribed pressure values. The insertion of the rigid inclusions in each step is done by removing points from the design space. The BEM model geometry is updated automatically using a weighted Delaunay triangularization algorithm capable of detecting 'holes' at those positions where the points have been eliminated.

The capabilities of the proposed strategy are demonstrated by solving some examples.

1 INTRODUCTION

Apart from functionality, the aspects of comfort have become increasingly important for users of almost any kind of product. As a result, today design processes take into account the acoustic properties of an object, i. e. its acoustic radiation. Especially for the case of objects acting as sound barrier it is desirable to minimize the radiation in certain directions.

The classical problem in acoustic design consists in finding the optimum geometric configuration of an object (say a sound barrier) to satisfy a given design objective for its radiation performance. A usual approach to tackle this problem is by means of shape optimization tools which consist in finding the optimal geometry within a class of domains having the same topology as the initial design, i.e., no holes are introduced in the optimization domain (Feijóo et al. (2004); Divo et al. (2003)). However, the most general approach is topological optimization tools, which allow not only changing the shape of the object but its topology via the creation of internal holes. Topological optimization tools are capable to deliver optimal designs with a priori poor information on the optimal shape of the body.

Among the available topology optimization tools (see for example Bendsoe and Sigmund (2002)) the topological derivative is used in this work. The topological derivative was firstly introduced by Ceá et al. (1974) by combining a fixed point method with the natural extension of the classical shape gradient. The basic idea behind the topological derivative is the evaluation of cost function sensitivity to the creation of a hole. In this way, wherever this sensitivity is low enough (or high enough depending on the nature of the problem) the material can be progressively eliminated. More recently, Novotny et al. (2003) introduced a novel procedure for the computation of the topological derivative for potential elasticity problems. That approach was implemented within the boundary element method (BEM) framework for two-dimensional potential problems by Cisilino (2006) and for two and three dimensional elasticity problems by Carretero Neches and Cisilino (2008) and Bertsch et al. (2010), respectively.

In acoustics, Feijóo (2004) proposed a method for imaging 'hidden' objects inversely via inverse scattering analysis using the topological derivative approach. In that case the cost function is the difference between a prescribed scattering pattern and the one measured when illuminating the hidden object by a planar wave travelling in a given direction. Starting from an empty optimization domain, the topological derivative indicates the positions where to place rigid inclusions to produce a scattered field which will converge to the prescribed one.

Due to the inherent characteristics of its formulation, the BEM is a particularly effective tool to cover acoustic problems, e. g. Wrobel and Aliabadi (2002). Within the BEM context, this work presents a method which extends the topological derivative proposed by Feijóo (2004) to iteratively optimize the geometrical configuration of preexistent objects in order to fulfill an arbitrary objective on its scatter pattern. The focus of this work is strictly two-dimensional.

The following section will introduce the forward and the inverse problem, followed by an explanation of the topological derivative approach. Then the iterative process introduced is this work is described. A number of examples will be given to verify the method and to show some applications. An outlook is provided in the concluding remarks.

2 THE FORWARD AND THE INVERSE SCATTERING PROBLEMS

Following Feijóo (2004), the setting of the problem is depicted in Figure 1, where Ω is a homogeneous medium with scatters Ω_0 with boundary Γ_0. The boundary Γ_s is where the measurements of the scattering pattern are obtained and is assumed to be a circle of radius R_s that encloses all the scatterers.

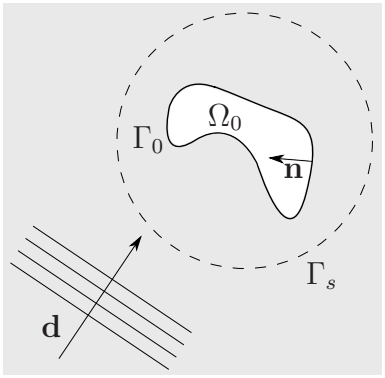

Figure 1: The inverse scattering problem according to Feijóo (2004)

The so-called *forward problem* describes the interaction between the medium, scatterers and the incident plane sound pressure wave $p_{inc}(\mathbf{x}) = e^{i\kappa\mathbf{x}\mathbf{d}}$ with propagation direction $\mathbf{d}$ and wave number $\kappa = \omega/c$ (the relation of the angular frequency ω to the speed of sound c) governed by the Helmholtz equation as follows

$$\nabla^2 p(\mathbf{x}) + \kappa^2 p(\mathbf{x}) = 0 \ \text{ in } \ \Omega = \mathbb{R} \setminus \Omega_0 \tag{1}$$

$$\nabla p(\mathbf{x}) \cdot \mathbf{n} = 0 \ \text{ on } \ \Gamma_0 \tag{2}$$

$$\lim_{r\to\infty} \sqrt{r} \left(\frac{\partial p_s}{\partial n} - i\kappa p_s \right) = 0, \tag{3}$$

where p is the total wavefield given by the addition of the incident and scattered pressure fields $p = p_{inc} + p_s$, and i is the imaginary unit. Equation (2) is the sound-hard boundary condition which means that scatterers are modeled as rigid objects. Equation (3) is the Sommerfeld condition which is valid for the scattered part of the wavefield and implies that only outgoing waves are allowed at infinity. It is assumed that there is no attenuation in the medium, so $\Im(\kappa) = 0$.

At Γ_s measurements of p are obtained for different directions $\mathbf{d}_i$ of the incident wave, which will be denoted as $p_m(\mathbf{d}_i)$ (in the following development, $\mathbf{d}_i$ will be dropped to simplify the notation). The objective of the *inverse problem* is to determine the shape of the scatterers Ω_0 such that $p|_{\Gamma_s} = p_m$. This last condition is enforced via a least-squares-type solution of the form:

find $\hat{\Omega}$ such that

$$\hat{\Omega} = \arg\min(\Omega) \tag{4}$$

where

$$J(\Omega) = \frac{1}{2} \int_{\Gamma_s} |p - p_m|^2 d\Gamma \tag{5}$$

where p is the solution of Eq. (1)–(3). Thus, the inverse problem is now written in the form of a constrained optimization problem with Ω as the design variable and the forward problem in Eq. (1)–(3) as a constraint on the admissible scalar field p.

The strategy to solve the above problem starts from a domain that contains no scatterers. Then, the functional in Eq. (5) is changed to account for the modification of the domain by

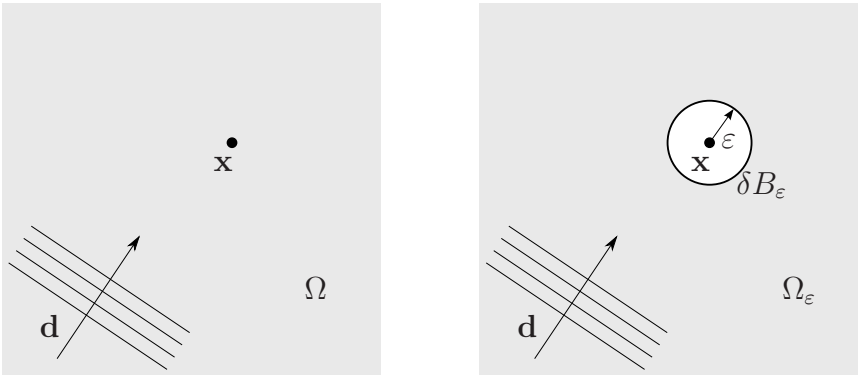

(a) $J(\Omega)$ (b) $J(\Omega_\varepsilon)$

Figure 2: Strategy for the solution of the inverse problem

introducing a small circular hole, $B_\varepsilon(\mathbf{x})$, centered at $\mathbf{x}$ and of radius ε. The new domain is denoted by $\Omega_\varepsilon = \Omega \setminus B_\varepsilon(\mathbf{x})$ (see Figure 2).

Denoting by $f(\varepsilon)$ the negative value of the 'size' of the hole B_ε, the new expression of the functional in Eq. (4) can be stated as follows:

$$J(\Omega_\varepsilon) = J(\Omega) + f(\varepsilon) D_T(\mathbf{x}) + \mathcal{O}\left(f(\varepsilon)\right), \tag{6}$$

where $D_T(\mathbf{x})$ is the topological derivative which measures the rate of change of the functional value with respect to the size of the scatterer $B_\varepsilon(\mathbf{x})$. The term $\mathcal{O}\left(f(\varepsilon)\right)$ is the remainder and satisfies

$$\lim_{\varepsilon \to 0^+} \frac{\mathcal{O}\left(f(\varepsilon)\right)}{f(\varepsilon)} = 0. \tag{7}$$

The scalar field $D_T(\mathbf{x})$ can be constructed by moving the point $\mathbf{x}$ in $\mathbb{R}^2$. Then the reconstruction technique can be motivated as follows: if it is necessary to choose where many small scatterers are to be placed in order to minimize the value of $J(\Omega)$ (and as a consequence recreate the shape of the scatterer by obtaining the scattering pattern that is close to p_m), they should be placed where D_T attains the highest values.

3 THE TOPOLOGICAL DERIVATIVE

The topological derivative $D_T(\mathbf{x})$ measures the sensitivity of a shape functional when an infinitesimal 'hole' is subtracted from the domain. This is defined through the following limit:

$$D_T(\mathbf{x}) = \lim_{\varepsilon \to 0} \frac{J(\Omega_\varepsilon) - J(\Omega)}{f(\varepsilon)} \tag{8}$$

where $f(\varepsilon)$ is a monotonically decreasing negative function such that $\lim_{\varepsilon \to 0} f(\varepsilon) = 0$. The selection of $f(\varepsilon)$, which corresponds to the size of the 'hole' but not necessarily is its measure in $\mathbb{R}^2$, is a non-trivial. The $f(\varepsilon)$ depends on the boundary condition specified on the surface δB_ε of the scatterer and it must satisfy $0 < |D_T(\mathbf{x})| < \infty$.

The direct application and implementation of the concept in Eq. (8) is not straightforward, as it is not possible to establish a homeomorphism between domains with different topologies (domains with and without the hole). A method for solving the problem using this approach for elasticity can be found in Garreau et al. (2001).

Many authors, and in particular Feijóo (2004) for the case of acoustic problems, proposed an alternative definition of the D_T that overcomes the above difficulties. They propose assimilating the creation of a hole to the perturbation of a pre-existing hole whose radius tends to zero (see Figure 3). Therefore, both topologies of the optimization domain are now similar and it is possible to establish a homeomorphism between them. According to this new definition, the expression for the D_T is

$$D_T(\mathbf{x}) = \lim_{\substack{\varepsilon \to 0 \\ \delta\varepsilon \to 0}} \frac{J(\Omega_{\varepsilon+\delta\varepsilon}) - J(\Omega_\varepsilon)}{f(\varepsilon+\delta\varepsilon) - f(\varepsilon)} \tag{9}$$

where $J(\Omega_\varepsilon)$ and $J(\Omega_{\varepsilon+\delta\varepsilon})$ are the cost functions evaluated for the reference and perturbed domain, ε is the initial radius of the hole, $\delta\varepsilon$ is a small perturbation of the hole radius and f is a regularization function. The function f is problem dependent and $f(\varepsilon) \to 0$ when $\varepsilon \to 0$.

It could be argued that the new definition of the D_T in Eq. (9) merely provides the sensitivity of the problem when the size of the hole is perturbed and not when it is effectively created (as it is the case in the original definition of the topological derivative). However, it is understood that to expand a hole of radius ε, when $\varepsilon \to 0$, is nothing more than creating it (a complete mathematical proof that establishes the relation between both definitions of the D_T is given in Novotny et al. (2003)). Moreover, the relationship between the two definitions constitutes the formal relation between the D_T and the shape sensitivity analysis. The advantage of the novel definition for the topological derivative given by Eq. (9) is that the whole mathematical framework developed for the shape sensitivity analysis can now be used to compute the D_T.

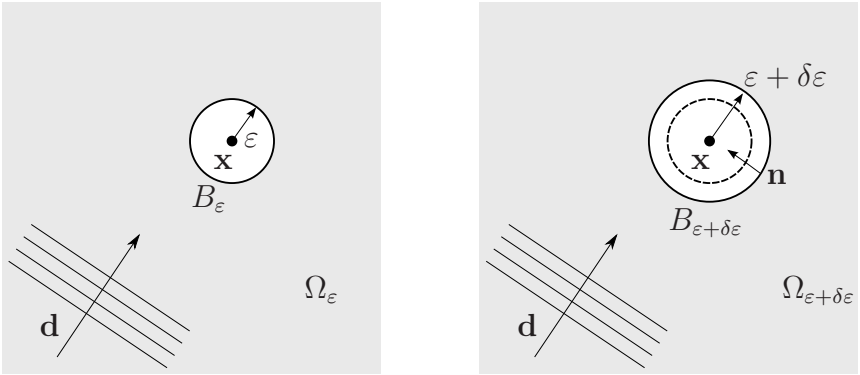

(a) $J(\Omega_\varepsilon)$ (b) $J(\Omega_{\varepsilon+\delta\varepsilon})$

Figure 3: Definition of the topological derivative using the shape sensitivity analysis approach

Among the available shape sensitivity analysis results, the differentiation of the shape derivative for acoustic problems presented by Feijóo et al. (2001, 2004) is of particular interest here. Given a shape functional $J(\Omega)$, the shape derivative $DJ(\Omega) \cdot \mathbf{V}$ in the direction given by the vector field $\mathbf{V}(x)$ is defined as follows:

$$DJ(\Omega) \cdot \mathbf{V} = \frac{d}{d\varepsilon} J\left(\phi_\varepsilon(\Omega)\right)|_{\varepsilon=0}, \tag{10}$$

where ϕ_ε is the mapping $\phi_\varepsilon(x) = x + \varepsilon \mathbf{V}(x)$ between the reference and perturbed domains. The computation of the shape derivative in Eq. (10) for the functional $J(\Omega)$ in Eq. (5) for the case in which the direction $\mathbf{V}(x)$ is that of the normal vector $\mathbf{n}(x)$ (see Figure 3) results in (a

detailed derivation of this result is in Feijóo et al. (2004)):

$$DJ(\Omega)\cdot\mathbf{V}=\Re\left[\int_{\Gamma_s}\left(\nabla\bar{\lambda}\cdot\nabla p-\kappa^2\bar{\lambda}p\right)v_n d\Gamma\right], \tag{11}$$

where p is the solution of the forward problem in Eq. (1)–(3) and λ is the solution of the following adjoint problem (the overbar symbol indicating the conjugate complex):

$$\nabla^2\lambda(\mathbf{x})+\kappa^2\lambda(\mathbf{x})=(p-p_m)(\mathbf{x})\delta_{\Gamma_s}\ \text{ in }\ \Omega \tag{12}$$

$$\nabla\lambda\cdot\mathbf{n}=0\ \text{ on }\ \Gamma_0 \tag{13}$$

$$\lim_{r\to\infty}\sqrt{r}\left(\frac{\partial\lambda}{\partial n}+i\kappa\lambda\right)=0. \tag{14}$$

In Eq. (12), δ_{Γ_s} is the Dirac delta-function defined on the sampling surface Γ_s. It should be noted that the adjoint field λ corresponds to the backpropagation (note the plus sign in Eq. (14) and compare with Eq. (3)) of the mismatch between the solution given by the forward model and the measured signature at Γ_s.

The topological derivative can be computed now by combining the results in Eq. (9) and Eq. (11). Having in mind that the boundary condition on ∂B_ε is the one of a rigid object (see Eq. (2)), it results

$$D_T(\mathbf{x})=-\lim_{r\to0}\frac{1}{f'(\varepsilon)}\Re\left[\int_{\partial B_\varepsilon}\left(\nabla\bar{\lambda_\varepsilon}\cdot\nabla p_\varepsilon-\kappa^2\bar{\lambda}_\varepsilon p_\varepsilon\right)d\partial B_\varepsilon\right], \tag{15}$$

where p_ε and λ_ε are solutions of the forward and adjoint problems posed in the configuration $\Omega_\varepsilon=\Omega\backslash B_\varepsilon(\mathbf{x})$. An asymptotic analysis of these solutions and their gradients at ∂B_ε reveals that these terms are of $\mathcal{O}(1)$ as $\varepsilon\to0$ (see Feijóo (2004)). Therefore, to satisfy $0<|D_T(\mathbf{x})|<\infty$ it is required that $f'(\varepsilon)=-2\pi\varepsilon$, which implies that $f(\varepsilon)=-\pi\varepsilon^2$. The final expression for the topological derivative is then

$$D_T(\mathbf{x})=\Re\left[2\nabla\bar{\lambda}(\mathbf{x})\cdot\nabla p(\mathbf{x})-\kappa^2\bar{\lambda}(\mathbf{x})p(\mathbf{x})\right], \tag{16}$$

where p and λ are solutions of the forward and adjoint problems. Feijóo (2004) applied this formulation to an empty domain which contains no scatterers. In his case the forward problem consists of a plane wave propagating undisturbed through the domain Ω while the adjoint problem is solved analytically. A BEM implementation for this kind of analysis was presented in a previous work by the authors (Cisilino et al. (2009)).

In this work, the scope of the topological derivative is extended to optimization domains containing an initial scattering object Ω_0. To this end, it is necessary to acquire the necessary solutions for the forward and adjoint problems necessary for the computation of D_T according to Eq. (16). These solutions are computed using the BEM. The details are given in the next section.

4 THE BOUNDARY ELEMENT IMPLEMENTATION FOR ACOUSTICS

In this work, the direct BEM formulation in the frequency domain is applied. The problem is governed by the Helmholtz-Equation (Eq. (17)) describing the (acoustic) pressure distribution

in a nonviscous compressible fluid. For sound propagation in an unbounded domain Sommerfeld's radiation condition (Eq. (18)) must be fulfilled additionally. This condition specifies that waves in an unbounded domain only travel into infinity. This is,

$$\nabla^2 p(\mathbf{x}) + \kappa^2 p(\mathbf{x}) = b(\mathbf{x}) \tag{17}$$

$$\lim_{r\to\infty} \sqrt{r}\left(\frac{\partial p}{\partial n} - i\kappa p\right) = 0 \tag{18}$$

where p is the acoustic pressure (the harmonic extention $e^{i\omega t}$ being omitted); b defines a source distribution; the sound flux $\partial p/\partial n$ is the partial derivative of pressure in normal direction and r the distance from the radiating surface.

To apply the BEM for a certain problem two prerequisites have to be fulfilled: the domain is homogeneous and the fundamental solution is known.

The fundamental solution describes the reactions in an unbounded domain caused by a point source with the intensity of 1 at point ξ. The fundamental solution needs to fulfill the inhomogeneous differential equation

$$\nabla^2 p^*(\mathbf{x},\xi) + \kappa^2 p^*(\mathbf{x},\xi) = -\delta(\mathbf{x}-\xi) \tag{19}$$

with $\delta(\mathbf{x}-\xi)$ being the Dirac delta function.

The fundamental solution p^* and its derivative $\partial p^*/\partial n = q^*$ (denoting the sound flux) are given in 2D by

$$p^*(\mathbf{x},\xi) = -\frac{i}{4} H_0^{(1)}(\kappa r) \;\text{ with }\; r := \mid \mathbf{x}-\xi \mid \tag{20}$$

$$\text{and}\quad q^*(\mathbf{x},\xi) = \frac{i\kappa}{4} H_1^{(1)}(\kappa r)\frac{\partial r}{\partial n}. \tag{21}$$

The boundary integral equation (BIE) is derived by applying the method of weighted residua to Eq. (17), using the fundamental solution as test function, applying Green's second identity and the filter function of the Dirac delta function. Then, moving the source point ξ to the boundary leads to the BIE:

$$c(\xi)p(\xi) + \int_\Gamma p(\mathbf{x})q^*(\mathbf{x},\xi))d\Gamma_x = \int_\Gamma q(\mathbf{x})p^*(\mathbf{x},\xi)d\Gamma_x + b(\xi). \tag{22}$$

The term $b(\xi)$ is the incident plain wave $p_{inc} = A\cdot e^{i\kappa\xi\mathbf{d}}$ at the point ξ, with A being the amplitude and $\mathbf{d}$ defining the propagation vector.

As an exact solution of the BIE is generally not available the boundary is discretized into a finite number of linear boundary elements, as depicted in Fig. 4 (left). The values for acoustic pressure p and flux q are approximated using shape functions in the form of $p = \mathbf{Np}$ and $q = \mathbf{Nq}$, respectively. The vector $\mathbf{N}$ holds the shape functions while $\mathbf{p}$ and $\mathbf{q}$ contain the values of pressure and flux at the nodes. Setting up the BIE (Eq. (22)) for each node (collocation method) leads to a system of equations

$$\mathbf{Gq} - \mathbf{Hp} = \mathbf{b} \tag{23}$$

where the matrices $\mathbf{G}$ and $\mathbf{H}$ contain the results of the integrals for shape functions and the fundamental solutions p^* and q^* along the element domains. It is worth noting here that since

the present application deals with sound-hard scatters only, the sound flux is always null along the complete model boundary. Thus, the system in Eq. (23) reduces to

$$-\mathbf{Hp} = \mathbf{b}, \tag{24}$$

which is used to compute the sound pressure p on the model boundary. Further details about the boundary element formulation and implementation can be found in any classic BEM book, e.g. Wrobel and Aliabadi (2002).

4.1 Computation of the forward fields

The computation of the D_T requires of the solution of the forward problem posted in Eq. (1)–(3) over the integration domain. To this end, and as it will be shown in next section, the present implementation makes use of a regular array of internal points following the pattern depicted in Fig. 4 (left).

Solving the forward problem in the BEM context gives in the first step the pressures p on the surface of the scatterer. In a second step the values of $p(\mathbf{x})$ are computed for all internal points within the design domain using the internal counterpart of the BIE introduced in Eq. (22). Recalling that the scatterer is considered as sound-hard, this is

$$p(\xi) = \int_\Gamma -p(\mathbf{x})q^*(\mathbf{x},\xi)d\Gamma + Ae^{i\kappa\xi\mathbf{d}} \quad \text{for} \quad \xi \in \Omega. \tag{25}$$

Similarly, the gradient $\nabla p(\mathbf{x})$ can be computed at the internal points using the space derivatives of Eq. (25) with respect to the internal points

$$\frac{\partial p(\xi)}{\partial x_i} = \int_\Gamma -p(\mathbf{x})\frac{\partial q^*(\mathbf{x},\xi)}{\partial x_i}d\Gamma + \frac{Ae^{i\kappa\xi\mathbf{d}}}{\partial x_i} \quad \text{for} \quad \xi \in \Omega. \tag{26}$$

Both $p(\mathbf{x})$ and $\nabla p(\mathbf{x})$ are essential inputs to compute the topological derivative $D_T(\mathbf{x})$, see Eq. (16).

4.2 Computation of the adjoint fields

The adjoint problem is given through Eq. (12)–(14). It is solved backwards using Eq. (25) without the influence of the incident wave:

$$(p - p_m)(\xi) = \int_\Gamma -\lambda(\mathbf{x})q^*(\mathbf{x},\xi)d\Gamma \quad \text{for} \quad \xi \in \Omega. \tag{27}$$

A system of equations is established in which the pressure values λ on the boundary of the scatterer are the unknowns. The points on the virtual surface Γ_s, for which the mismatch $(p - p_m)$ has been computed (see section 2), are regarded as internal points. In this way, Eq. (27) can be used to express the values at these points. Then, the unknown boundary values λ can be determined by setting up a system of equations using the aforementioned formula for the evaluation of internal points. The equation system is of the form

$$\begin{bmatrix} h_{11} & h_{12} & \cdots & h_{1n} \\ h_{21} & h_{22} & \cdots & h_{2n} \\ \vdots & \vdots & \ddots & \vdots \\ h_{N1} & h_{N2} & \cdots & h_{Nn} \end{bmatrix} \begin{bmatrix} \lambda_1 \\ \lambda_2 \\ \vdots \\ \lambda_n \end{bmatrix} = \begin{bmatrix} (p-p_m)_1 \\ (p-p_m)_2 \\ \vdots \\ (p-p_m)_n \end{bmatrix} \tag{28}$$

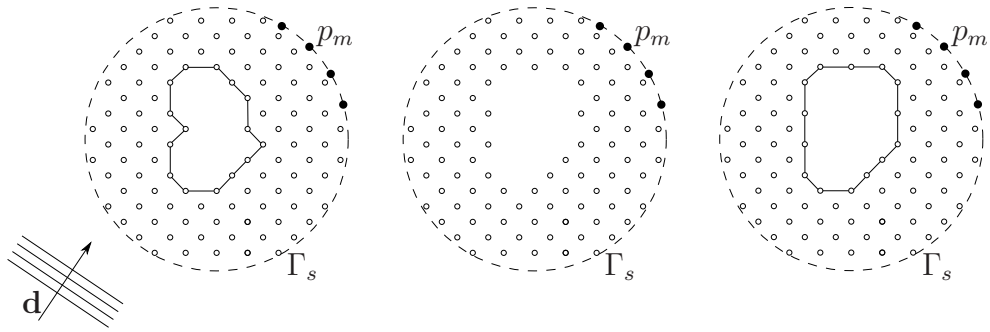

Figure 4: Remeshing of the BEM model: (left) initial BEM model, (middle) elimination of internal points, (right) BEM model after remeshing

where the components h_{ij} are made up of the integrals of the fundamental solution $q^* = \partial p^*/\partial n$; λ_i are the values of all n nodes forming the boundary of the scatterer and $(p-p_m)_i$ define the mismatch in pressure values of the N points along the virtual surface Γ_s. Using standard procedures (see Hampel et al. (2008)) the system of equations is constructed with $N = 3n$, i. e. the number of points along the virtual surface is three times the number of nodes discretizing the scatterer's boundary. A single value decomposition (SVD) algorithm is applied to solve the system of equations of Eq. (28).

Having acquired the solution λ on the boundary of the scatterer, the values of $\lambda(\mathbf{x})$ and $\nabla\lambda(\mathbf{x})$ for all internal points are determined using the same procedure as described for the forward problem. To solve for $\lambda(\mathbf{x})$ Eq. (27) is applied, while the according formula for $\nabla\lambda(\mathbf{x})$ is given by

$$\frac{\partial\lambda(\xi)}{\partial x_i} = \int_\Gamma -\lambda(\mathbf{x})\frac{\partial q^*(\mathbf{x},\xi)}{\partial x_i}d\Gamma \quad \text{for} \quad \xi \in \Omega. \tag{29}$$

5 THE ITERATIVE PROCESS

Feijóo (2004) employs in his work the method of the topological derivative only once to determine the most probable shape of an unknown scattering object. In this work an iterative approach is proposed to find the optimal shape of a scatterer which fulfills best to a set of prescribed values at certain points (e. g. along a circle surrounding the design space). To start the iterative process an initial scatterer is placed into the design domain which will grow with each iterative step until the shape considered optimal is reached. To this end, the procedure presented in Cisilino (2006) and Carretero Neches and Cisilino (2008) is used.

Having checked the stopping criterion (typically a limit value h for the difference $p - p_m$, hence testing $p - p_m < h$) and finding that it is not fulfilled (p has been computed for a given configuration, see Fig. 4 (left)), the iterative process consists of the following steps:

1. Computing the pressure field $p(\mathbf{x})$ and its gradient $\nabla p(\mathbf{x})$ for all internal points and points along the virtual surface Γ_s
2. Determining the mismatch between the solution of the forward problem p and the prescribed values p_m at the virtual surface Γ_s: $(p - p_m)$
3. Solving the adjoint problem (Eq. (12)–(14)) to obtain the pressure field λ, see Fig. 4 (left)
4. Computing the pressure field $\lambda(\mathbf{x})$ and its gradient $\nabla\lambda(\mathbf{x})$ for all internal points
5. Computing the topological derivative $D_T(\mathbf{x})$ using Eq. (16)

6. Eliminating those internal points with the maximum values of D_T (in general a small percentage of points), see Fig. 4 (middle)

7. Remeshing the BEM model, see Fig. 4 (right)

8. Solving the forward problem (Eq. (1)–(3)) for incident plane waves for the new configuration using the BEM

9. Checking the stopping criterion, if necessary, repeating from step 1

The final geometry is obtained once the checking criterion is fulfilled.

To overcome the difficulties when evaluating $D_T(\mathbf{x})$ for points on the boundary Γ_0 of the scatterer a workaround is proposed. Instead of determining the topological derivative for a point directly on the scatterer's boundary, the topological derivative is computed for a point that is within the design domain at a small distance from the boundary node. The chosen distance is much smaller than the regular spacing between points in the design space. The topological derivative for this auxiliary point is then mapped onto the corresponding node on the scatterer's boundary. It is worth noticing that not defining the topological derivative D_T on the scatterer's boundary Γ_s would lead to the elimination of all points of the boundary in each iterative step. This would cause falsified growth of the scatterer leading to wrong results.

5.1 Model discretization and remeshing

The model discretization and remeshing strategies are key issues for the performance of the implemented algorithm. The initial BEM model is discretized using two-node linear elements and a regular array of internal points following the pattern depicted in Figure 4. The removal of internal and boundary points in every increment is followed by a model remeshing. With this purpose the program *MeshSuite*, based on an α-shapes algorithm, is employed (Calvo et al. (2003)). Alpha shapes can be viewed as Delaunay triangularization of a point set weighted by the parameter α. Alpha shapes formalize the intuitive notion of shape, and for varying parameter α, it ranges from crude to fine shapes. The most crude shape is the convex hull itself, which is obtained for very large values of α. As α decreases, the shape shrinks and develops cavities that may join to form holes. In this work the parameter α is selected as the average distance between boundary nodes. This is the reason why internal points are distributed on the model domain using a regular array. Upon the input of the coordinates of the boundary nodes and internal points after each optimization step (see Fig. 4 (middle)), *MeshSuite* outputs the connectivity of the new model boundary (see Fig. 4 (right)). Thus, those points not used as boundary nodes are assimilated to internal points in the new discretization.

Depending on the spatial distribution of the points, multi-connected boundary points which take part in the connectivity of two (or even more) boundaries could arise. This problem is remedied by simply removing the conflicting points from the model. Multi-connected points are identified after checking that every valid boundary node belongs to the connectivity of two boundary elements only.

6 EXAMPLES

Results for two examples are presented in this section. In order to assess the performance of the iterative method, the first example is a validation example while the second one conisists in an application problem.

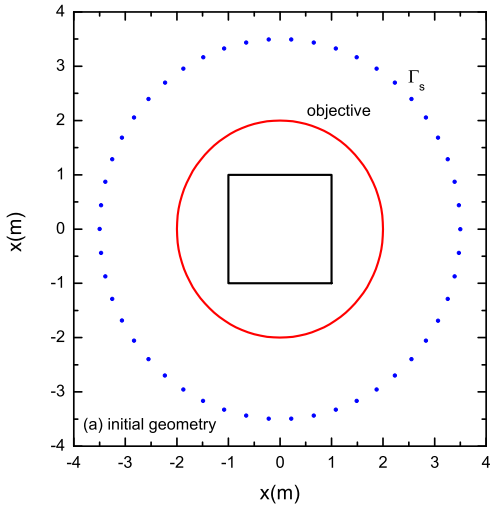

Figure 5: Problem set-up for the validation example

6.1 Reconstruction of a circular scatterer

This first example consists in the reconstruction of a circular scatterer of radius $R = 2m$ starting from a square initial geometry of side $L = 2m$, see Fig. 5. The initial geometry is discretized using 160 elements. The optimization domain is a square of size $6m\ x\ 6m$ discretized using 13639 internal points which are placed on a square grid with a step $l = 0.05m$. The size of the grid is also the length of the elements in the BEM discretization. The element length was selected to be approximately four times smaller than the wave length.

The objective values, p_m, along the virtual surface Γ_s is the scattered field for the circular object when it is illuminated by 100 planar sound waves (the angle of incidence equally distributed over 2π) with a wavenumber $\kappa = 32\ m^{-1}$ and an amplitude $A = 1\ Pa$. The objective values are specified at $N = 800$ points evenly distributed along Γ_s. This large number of points guarantees the fulfillment of the condition $N = 3n$ when solving the adjoint problem (see Eq. (28)) during the complete optimization procedure.

The topological derivative is computed by adding up the solutions obtained for all the incident waves. Scatterers are placed (or in other words, internal points are removed) at the positions of the internal points with the highest values for the topological derivative. For this example the internal-point removal rate is chosen equal to 2.5% of the current number of internal points in the model per step, so that the number of internal points eliminated in each optimization step diminishes as the algorithm progresses. This strategy helps the algorithm to converge towards the optimum solution.

Figures 6(a) and 6(b) illustrate contour plots for the pressure solutions p and λ for the direct (Eq. (1)–(3)) and adjoint problems (Eq. (12)–(14)) for the initial geometry illuminated by a wave travelling in x direction. The topological derivative field after computing Eq. (16) is plotted in Fig. 7(a) for the same wave and in Fig. 7(b) for the summation over all the 100 waves. It can be seen that maximum values for the D_T are situated around the initial boundary. It is from those zones that the internal points are removed to update the geometry of the scatterer for the second step. The resulting geometries for the subsequent steps are plotted in Fig. 9.

Figure 8 shows the objective and current pressure values along the virtual surface Γ_s for se-

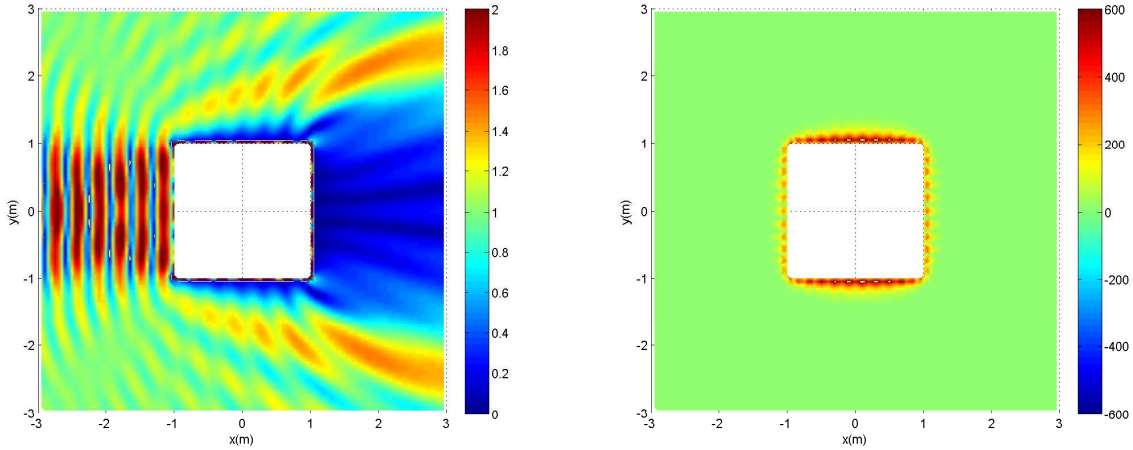

(a) Solution p of the forward problem (b) Solution λ of the adjoint problem

Figure 6: Pressure wavefield for the forward and the adjoint problem for a wave travelling in x direction

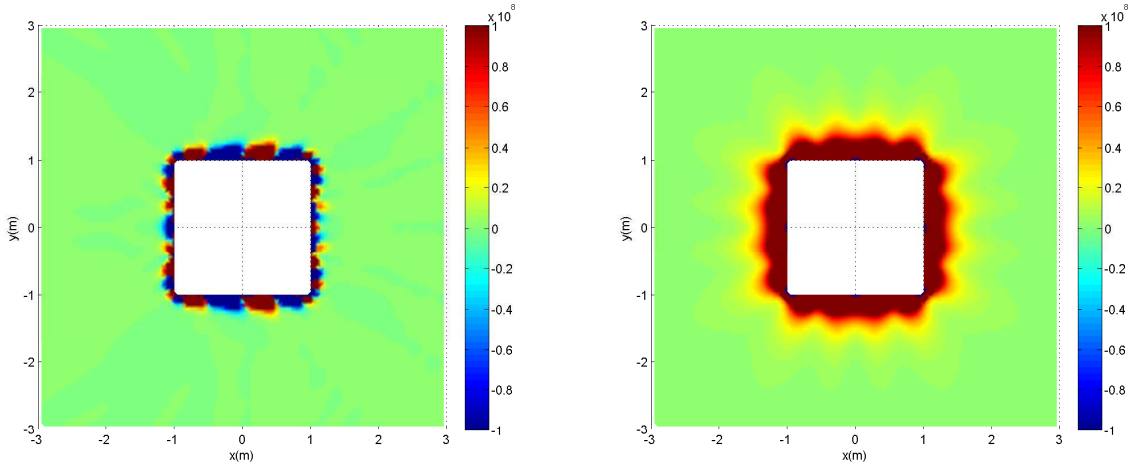

(a) for one incident wave travelling in x direction (b) summarized over all 100 incident waves

Figure 7: Topological derivative fields D_T

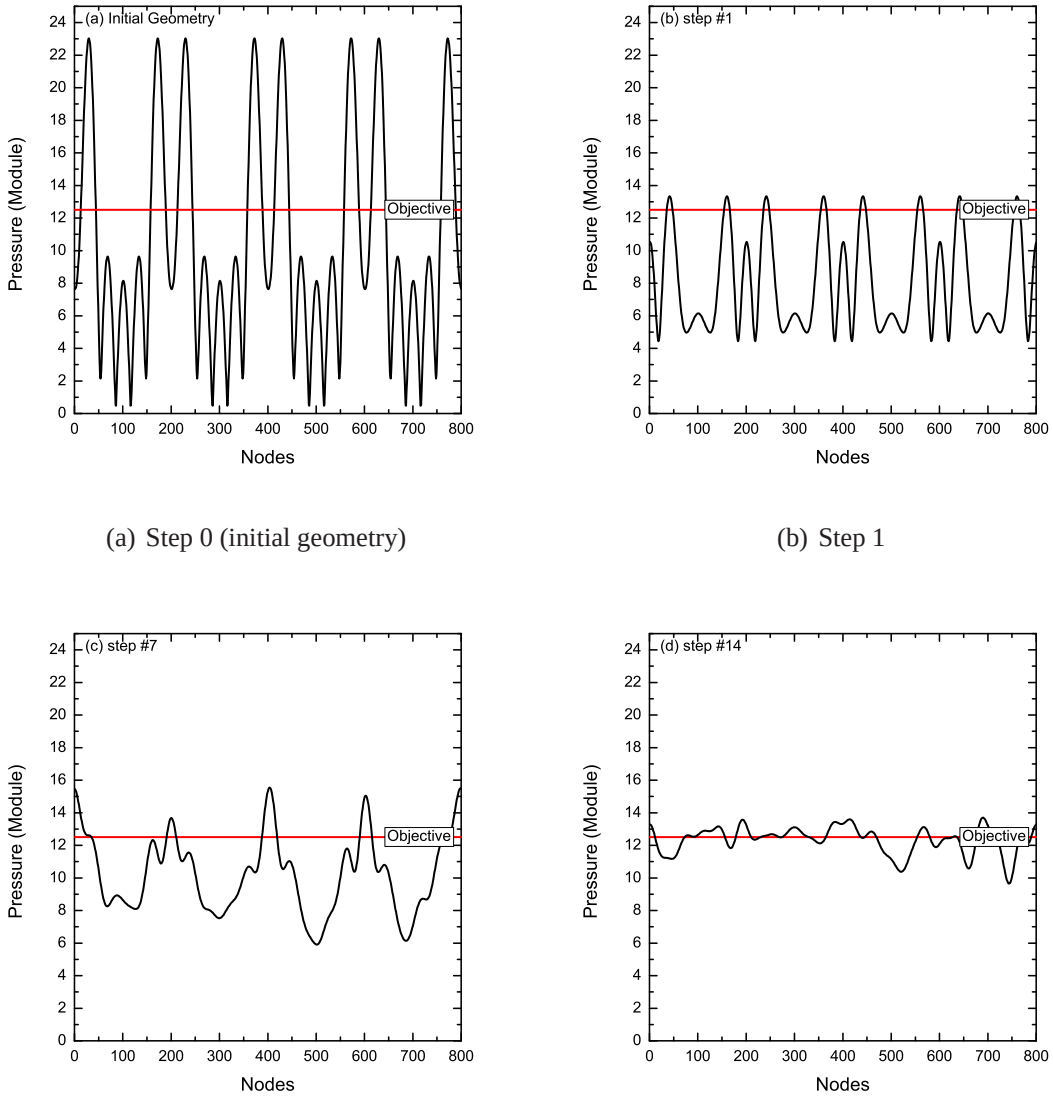

(a) Step 0 (initial geometry)

(b) Step 1

(c) Step 7

(d) Step 14

Figure 8: Evolution of the objective and current pressure values along the virtual surface Γ_s for selected iteration steps

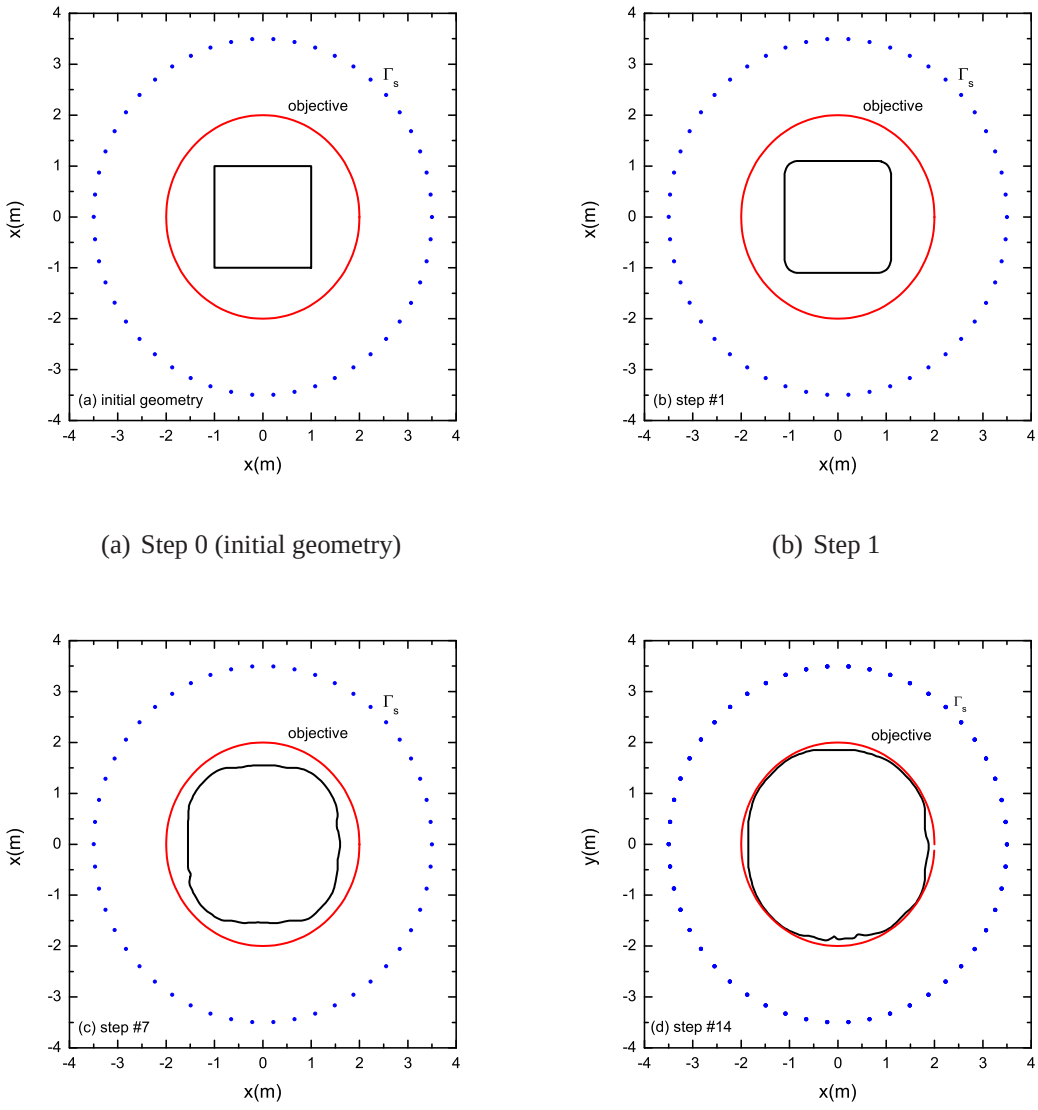

(a) Step 0 (initial geometry)

(b) Step 1

(c) Step 7

(d) Step 14

Figure 9: Development of the scatterer's geometry for selected iteration steps

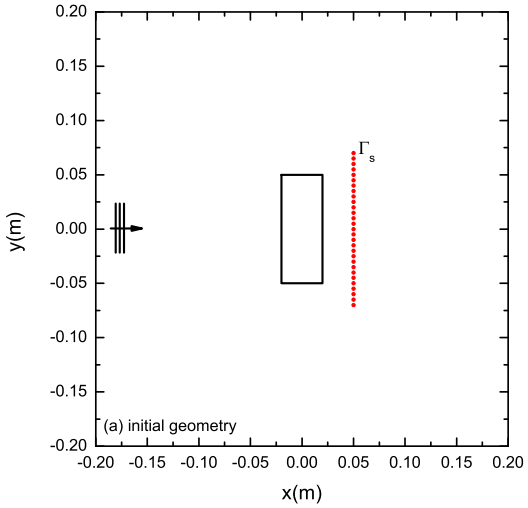

Figure 10: Problem description for the second example (zero pressure on Γ_s)

lected iteration steps. The depicted pressures are the summation of the values p of the scattered fields at Γ_s for all 100 incident waves. It can be seen from Fig. 8 and 9 that the pressure results converge towards their objective values as the shape of the scatterer approaches that of a circle.

6.2 Creating a barrier for a zero pressure zone

This example consists of the optimization of the geometry of a barrier in order to get zero pressure (considering both the incident and the scattered fields) behind it when it is illuminated by a single plane wave travelling in the x direction, see Fig. 10. The initial geometry of the barrier is a rectangle with dimensions $0.1m\ x\ 0.04m$ and with its barycenter in the position $x = 0$, $y = 0$. The zero pressure objective is specified along a line at $x = 0.05m$, ranging from $y = -0.07m$ to $y = 0.07m$ (being this virtual surface Γ_s).

The wavenumber of the incident wave is $\kappa = 32\ m^{-1}$ and its amplitude is $A = 1\ Pa$. The optimization domain is a square of size $1m\ x\ 1m$ discretized using 13639 internal points placed on a square grid with a step $l = 0.01m$. The initial geometry of the barrier is discretized using 28 elements. Eight hundred points are equidistantly placed along the surface Γ_s. The internal-point removal rate is chosen equal to 0.5 % of the current number of internal points per step.

Figure 11 shows the evolution of the pressure results along the Γ_s with the optimization process. For each case the resulting pressure values are plotted together with the objective values (zero pressure). The geometry for the last step computed is given in Fig. 12. The results in Figure 11 show the effectiveness of the optimization procedure to achieve the zero pressure objective along Γ_s.

7 CONCLUSION

The work presented here proposes an iterative optimization method using the topological derivative framework and the BEM. The given approach is capable to determine the shape of a scattering object which fulfills to prescribed pressure values on a virtual surface which surrounds the design domain. Considering the given examples it can be concluded that the

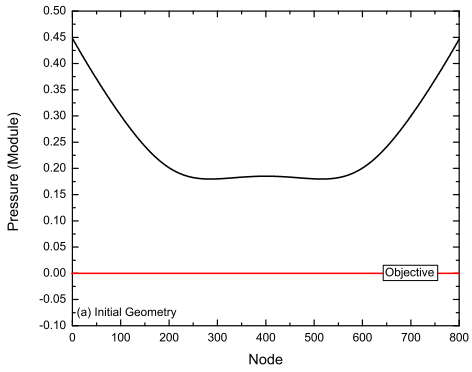

(a) Step 0 (initial geometry)

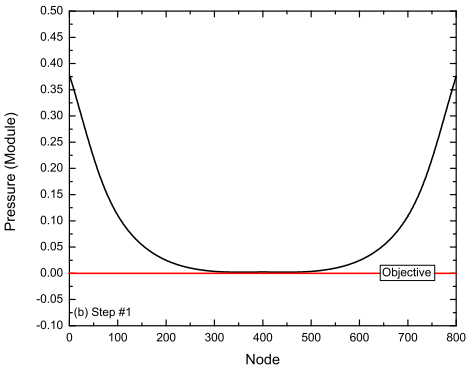

(b) Step 1

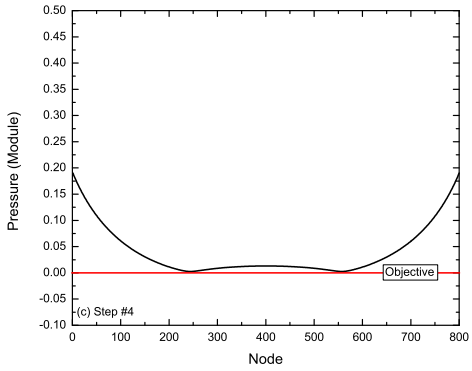

(c) Step 4

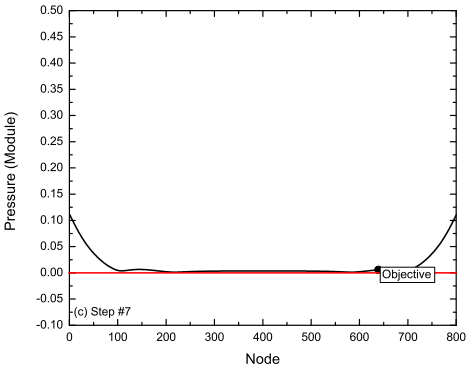

(d) Step 7

Figure 11: Pressures along Γ_s for different iteration steps

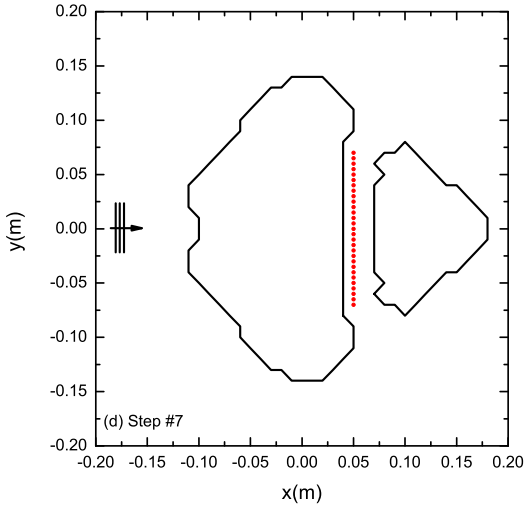

Figure 12: Geometry of the scatterer acquired after Step 7

proposed iterative method is an effective approach to find the optimal shape of a scatterer.

The discretization and remeshing procedures employed here handle well configurations of arbitrary shape. However, geometric irregularities on the scatterer's boundary may appear due to the spatial distribution of the internal points in the design domain. These can have a serious effect on the results. To avoid these effects smoothing should be performed to ensure the performance of the proposed method.

Further studies are intended to examine the effectiveness of the method when the objective values result from concave scatterers. It is assumed that in those cases special care has to be taken of the smoothing algorithm in order not to straighten out the concave features. Another topic of interest is the determination of the optimal shape of sound barriers when the design space is limited or predefined, which is most often the case for practical applications.

ACKNOWLEDGEMENTS

This work has been supported by the project DA 0806 sponsored by Ministerio de Ciencia, Tecnología e Innovación Productiva (MINCYT, Argentina) and Deutscher Akademischer Austauschdienst (DAAD, Germany).

REFERENCES

Bendsoe M.P. and Sigmund . *Topology Optimization*. Springer, Berlin, 2002.

Bertsch C., Cisilino A.P., and Calvo N. Topology optimization of 3d elastic structures using boundary elements and the topological derivative. *Advances in Engineering Software*, 41:694–704, 2010.

Calvo N., Idelsohn S.R., and Oñate E. The extended delaunay tessellation. *Engineering Computations*, 20(5–6), 2003.

Carretero Neches L. and Cisilino A.P. Topology optimization of 2d elastic structures using boundary elements. *Engineering Analysis with Boundary Elements*, 32:533–544, 2008.

Ceá J., Gioan A., and Michel J. Adaptation de la méthode du gradient a un problème d'idenfification de domaine. In *Lecture Notes in Computer Science*, volume 11, pages 371–402. Springer, Berlin, 1974.

Cisilino A.P. Topology optimization of 2d potential problems using boundary elements. *Computer Modelling in Engineering & Sciences*, 15(2):99–106, 2006.

Cisilino A.P., Beck S., and Langer S. Reconstruction analysis for inverse scattering using the topological derivative and the boundary element method. In *XVIII Congreso sobre Métodos Numéricos y sus Aplicaciones ENIEF2009*. Tandil, 2009.

Divo E.A., Kassab A.J., and Ingber M.S. Shape optimization of acoustic scattering bodies. *Engineering Analysis with Boundary Elements*, 27(7):695–703, 2003. Special issue on Acoustics.

Feijóo G.R. A new method in inverse scattering based on the topological derivative. *Inverse Problems*, 20:1819–1840, 2004.

Feijóo G.R., Malhotra M., Oberai A.A., and Pinsky P.M. Shape sensitivity calculations for exterior acoustics problems. *Eng. Comput.*, 18:376–391, 2001.

Feijóo G.R., Oberai A.A., and Pinsky P.M. An application of shape optimization in the solution of inverse acoustic scattering problems. *Inverse Problems*, 20:199–228, 2004.

Garreau S., Guillaume P., and Masmoudi M. The topological asymptotic for pde systems: the elasticity case. *SIAM J. Control Optim.*, 39:1756–78, 2001.

Hampel S., Langer S., and Cisilino A.P. Coupling boundary elements to a ray tracing procedure.

International Journal for Numerical Methods in Engineering, 73(3):427–445, 2008.
Novotny A.A., Feijoo R.A., Taroco E., and Padra C.C. Topological sensitivity analysis. *Comput Methods Appl. Mech. Eng.*, 192:803–829, 2003.
Wrobel L. and Aliabadi F. *The Boundary Element Method, Applications in Thermo-Fluids and Acoustics*, volume 1. John Wiley & Sons, 2002.